



Optimization methodology to study/estimate permeability in reverse osmosis desalination

Muhammad Bilal Minhas, Woo-Seung Kim*

Department of Mechanical Engineering, Hanyang University, 55 Hanyangdaehak-ro, Sangnok-gu, Ansan Kyeonggi-do 426-791, Korea, Tel. +82 31 400 5248; Fax: +82 31 418 0153; email: wskim@hanyang.ac.kr

Received 2 August 2013; Accepted 27 February 2014

ABSTRACT

In order to establish a method for the prediction of permeability, the significance of permeability in simulating a reverse osmosis (RO) module is studied. An optimization methodology incorporating the simulation model was established to estimate the water and salt permeability, and a number of correlations were studied to represent them. Optimized correlations were then validated over a wide range of operating conditions for a typical RO system for seawater desalination (50–80 bar, 20–35 °C, and 25–40 kg m⁻³). Using these permeability correlations, the model satisfactorily predicted two different published experimental observations: (1) predicted the permeate flow rate within a 5% error for 88% of the readings and the permeate concentration within a 10% error for 92% of the readings, and (2) predicted the permeate flow rate within a 6.2% error for 94% of the readings and the permeate concentration within an 8% error for 91% of the readings. The relative deviation between the experimental and predicted results using this procedure is 56% less than the published predicted result. Thus, a method to reliably determine a single permeability correlation for each of the water and salt permeability was established.

Keywords: Permeability; Desalination; Reverse osmosis; Simulation; Optimization

1. Introduction

The purpose of desalination is the production of low-salt freshwater from saline water. Among the various desalination technologies, multi-stage flash (MSF), reverse osmosis (RO), and multiple-effect distillation (MED) are likely to dominate in the future [1]. MSF and MED are distillation-based desalination processes and require heating, while in RO thermal energy is not required. RO technology is a feasible and prominent desalination method for water supply

[2], around half of the total desalination investment is in seawater RO [3]. There is a continuous progress in the improvement of membranes [4], also in the desalination techniques [5–7] to improve cost-effective water production and water recovery.

There are four types of membrane modules: plate and frame, tubular, spiral wound, and hollow fiber. Currently, the spiral-wound module (SWM) dominates the market. The feed solution mixes well in SWM due to continuous change of flow. A typical SWM has a

*Corresponding author.

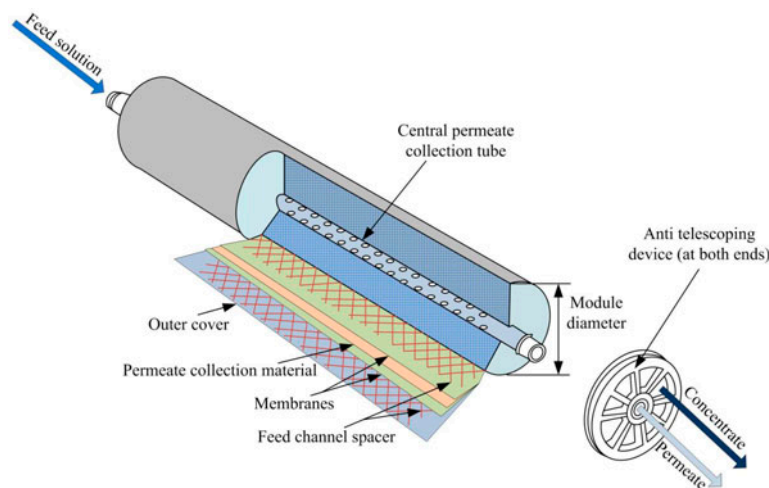


Fig. 1. Schematic of a typical SWM.

packing density of $\sim 250 \text{ m}^2/\text{m}^3$, and flow channel¹ size of $\sim 0.05 \text{ cm}$ [8]. The schematic of a SWM is shown in Fig. 1.

Although there are many proposed models for transport through RO membranes, mathematical/numerical models are principally based on either a solution diffusion model such as in [9–11] or a Spiegler and Kedem model [8,12]. Much work related to performance predictions in the desalination process by SWMs is available in the literature [8–11,13]. In RO membranes water flux is a function of permeability along with feed, and osmotic pressure [14], and permeability is a topic of interest for many recent researchers [15,16]. Solute and solvent permeability is the fundamental membrane parameter to simulate the flow through membrane, and cannot be measured directly, so indirect determination is required.

For the estimation of water and salt permeability, Sundaramoorthy et al. [11] developed a graphical linear fit method that included the following: pressure drop in the feed channel, transmembrane pressure, feed flow, retentate flow, module length and width, and feed channel friction parameter. Avlonitis et al. [9] united the pressure effect with the Arrhenius type equation for solute permeability to find the correlation in terms of pressure, and temperature. For salt permeability, the same authors Avlonitis et al. [17] determined the regression-based equation in terms of the temperature only. Voros et al. [18] used the non-dimensional form of the operating conditions (pressure, mole fraction) for the permeability, and selected

the optimum correlation through a simple regression procedure. By plotting the net driving force vs. the permeate water flux and the solute concentration difference across the membrane vs. permeate side salt flux Hung et al. [2] determined water and salt permeability, respectively, by the slopes. Permeability of water and salt was related to temperature using Arrhenius type equation [19]. Taking a different approach from others, Senthilmurugan et al. [8] determined the values of water and salt permeability for specific temperatures but independent of the operating pressure.

The accuracy of prediction of a model depends on the suitability of parameter. However, the permeability in all the above-referred studies was estimated using diverse approaches by relating permeability with different parameters. The accuracy of prediction of a model depends upon the suitability of parameter. A representative unique method that can be used to estimate permeability (parameter) in any type of membrane/module is vital. In addition to this, a single permeability correlation for each of the water and salt permeability is needed to reliably predict the permeability under varying operating conditions. Optimization methodology was established to study/predict the permeability trends/behavior under the effect of operating conditions. The correlation for the water permeability is associated with temperature and pressure, while the salt permeability correlation is associated with temperature, pressure, and concentration. With this procedure, various permeability correlations were studied for the water and the salt permeability—from these correlations one suitable correlation for the salt permeability and the other correlation for the

¹Flow channel is the path for feed to flow between the membranes and it is much smaller than module diameter (please refer to Figs. 1 and 2).

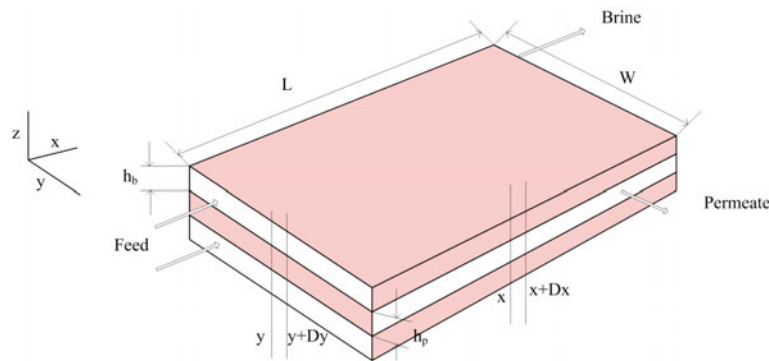


Fig. 2. Flow path and dimensions of conceptually unwound SWM [8].

water permeability was determined. The suitability of the correlation is based on the extent it fits the experimental data [10].

2. Model equations and outline

2.1. Model equations

This study is based on the model developed by Senthilmurugan et al. [8], which is based on the Spiegler and Kedem model. In an unwound SWM, there are two membrane sheets in a single leaf, and between the membranes is a permeate channel (see Fig. 2). In order to simulate the SWM, many researchers have conceptually considered the membrane as unwound. The formulated numerical models based on this assumption could well simulate the experimental data [8,11,19]. In the present study, the same approach is adopted to simulate the SWM as shown in Fig. 2. Theoretically, each sheet is divided into 11×21 (i.e. $m = 11$ parallel to brine flow direction, x axis, $n = 21$ parallel to the permeate flow direction, y axis).

$$S_{ij} = \frac{2(L \times W)}{(m \times n)} \quad (1)$$

$$\Delta x = \frac{L}{m} \quad (2)$$

$$\Delta y = \frac{W}{n} \quad (3)$$

where the membrane surface area is S [m^2 ; L^2], with length L [m ; L], and width W [m ; L], while ij are the nodes of the index along the length, and width of the

membrane, respectively. The size of each sub division along the x, y axis, respectively is, Δx and Δy [m ; L].

Volumetric water flux $J_{v,ij}$ [$m^3 m^{-2} s^{-1}$; $L T^{-1}$] through the membrane is:

$$J_{v,ij} = A[(P_{b,ij} - P_{p,ij}) - \sigma\alpha\phi_{i,j}(C_{b,ij} - C_{p,ij})] \quad (4)$$

where A is the water permeability [$m^3 m^{-2} s^{-1} Pa^{-1}$; $L T^{-1}$], P is the hydraulic pressure [Pa ; $ML^{-1} T^{-2}$], C is the solute concentration [$kg m^{-3}$, ML^{-3}], (subscripts $b =$ feed side, $p =$ permeate side), α is the osmotic pressure proportionality [$m^3 Pa kg^{-1}$; $L^2 T^2$], σ is the reflection coefficient. Here, $\alpha = 2RT$ (R being ideal gas constant and T is temperature) [8]. The equations for the concentration polarization effect $\phi_{i,j}$ is expressed as:

$$\phi_{i,j} = \frac{C_{m,ij} - C_{p,ij}}{C_{b,ij} - C_{p,ij}} = \exp\left(\frac{J_{v,ij}}{k_{i,j}}\right) \quad (5)$$

(Subscript $m =$ membrane feed interface) and k is mass transfer coefficient [$m s^{-1}$; $L T^{-1}$]

The solute concentration in the permeate stream C_p can be expressed as:

$$C_{p,ij} = [\phi_{i,j}(1 - R_{i,j})C_{b,ij}]/[\phi_{i,j} + R_{i,j}(1 - \phi_{i,j})] \quad (6)$$

The concentration on the feed/brine side C_b , and brine rejection rate R are:

$$C_{b_{i+1,j}} = \frac{1}{Q_{b_{i+1,j}}} (C_{b,ij} Q_{b_{i,j}} - S_{i,j} C_{p,ij} J_{v,ij}) \quad (7)$$

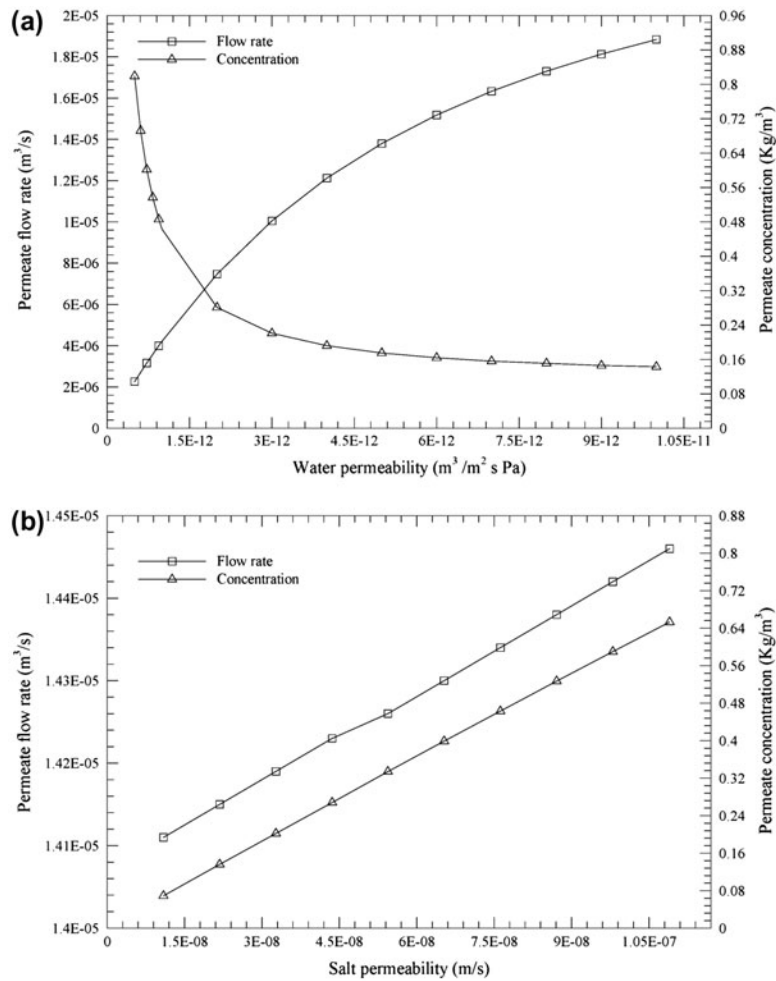


Fig. 3. Effect of permeability on permeate characteristic prediction of numerical model. Permeate water flow rate and permeate concentration as a function of (a) water permeability and (b) salt permeability.

$$R_{i,j} = \frac{(1 - F_{i,j})\sigma}{1 - \sigma F_{i,j}} \tag{8}$$

where $F_{i,j} = \exp(-Jv_{i,j}(1 - \sigma)/B)$ and Q_b is brine flow rate calculated as:

$$Q_{b,i,j} = \frac{Q_f}{(n \times \text{leaves})} \tag{9}$$

$$Q_{b,i+1,j} = Q_{b,i,j} - J_{v,i,j} S_{i,j} \tag{10}$$

where Q_f is initial flow rate at inlet [$m^3 s^{-1}$; $L^3 T^{-1}$] and leaves represents the number of membrane leaves in the module.

The initial and boundary conditions used in this study are as follows:

Feed side:

$$\left. \begin{aligned} P_{b,i,1} &= P_f \\ U_{b,i,1} &= U_{f,i,1} \\ U_{b,i,1} &= q_{b,i,1}/(h_b \Delta y) \\ C_{b,i,1} &= C_f \end{aligned} \right\} \text{ for } i = 1 \text{ to } m \tag{11}$$

Permeate side:

$$\left. \begin{aligned} \frac{dP_{p1,j}}{dy} &= 0 \\ U_{p,m,j} &= 0 \\ \frac{dC_{p1,j}}{dy} &= 0 \\ P_{p,m,j} &= 1 \text{ atm} \end{aligned} \right\} \text{ for } j = 1 \text{ to } n \tag{12}$$

The hydraulic pressure drop in the feed channel and the permeate channel along the x and y axis, respectively, were estimated based on Darcy’s law as follows:

$$P_{b_{i-1,j}} - P_{b_{i,j}} = 2\Delta x^2 \mu k_{fb} \sum_{l=1}^{i-1} \left(\frac{J_{v,l,j}}{h_b} \right) \quad (13)$$

$$P_{p_{i,j+1}} - P_{p_{i,j}} = 2 k_{fp} \mu \Delta y^2 \sum_{l=j+1}^n \left(\frac{J_{v,i,l}}{h_p} \right) \quad (14)$$

where k_{fb} and k_{fp} are the friction parameters for the feed channel and the permeate channel respectively [$m^{-2}; L^{-2}$], h_p is the permeate channel height [m; L].

Finally, the total permeate flow Q_{pt} [$m^3 s^{-1}; L^3 T^{-1}$] and average permeate concentration C_{pt} [$kg m^{-3}; ML^{-3}$] are estimated as follows:

$$Q_{pt} = N_L \left(\sum_{i=1}^m \sum_{j=1}^n (J_{v,i,j} S_{i,j}) \right) \quad (15)$$

$$C_{pt} = \frac{N_L}{Q_{pt}} \left(\sum_{i=1}^m \sum_{j=1}^n (C_{p_{i,j}} J_{v,i,j} S_{i,j}) \right) \quad (16)$$

where N_L is the number of membrane leaves in one module.

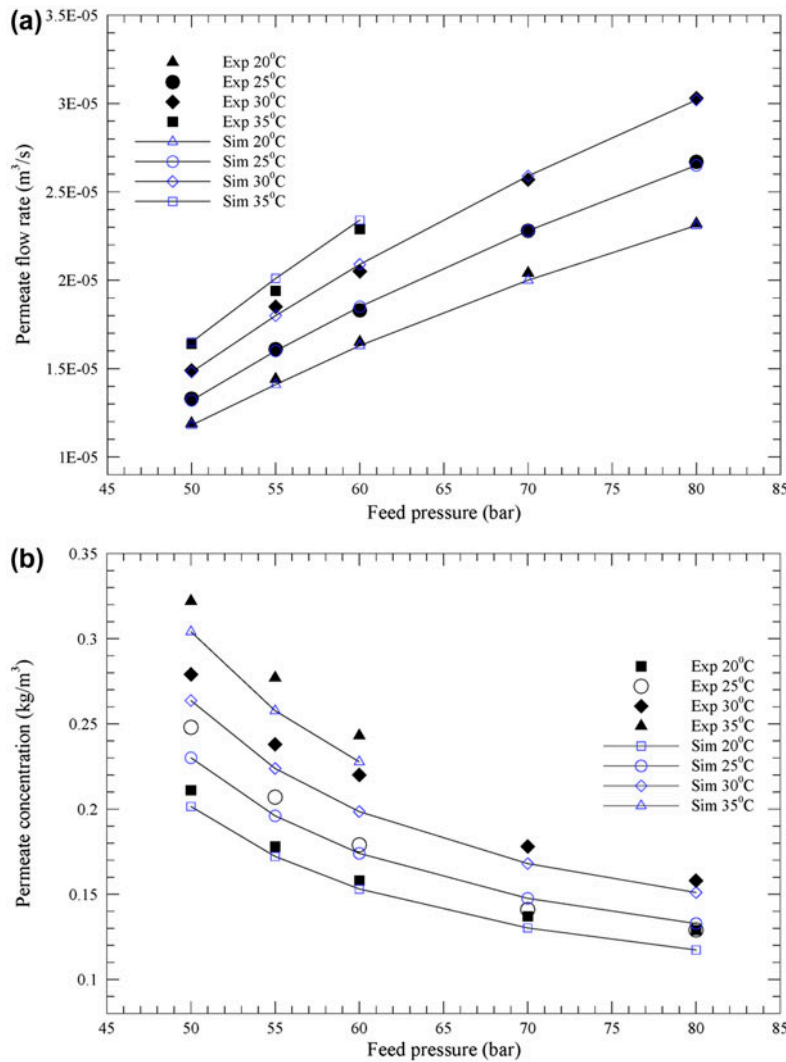


Fig. 4. Permeate characteristics of Boudinar’s [10] experimental data, predicted using permeability correlations Eqs. (23) and (24); (a, b) $C_f = 35 kg m^{-3}$ and (c, d) $C_f = 40 kg m^{-3}$.

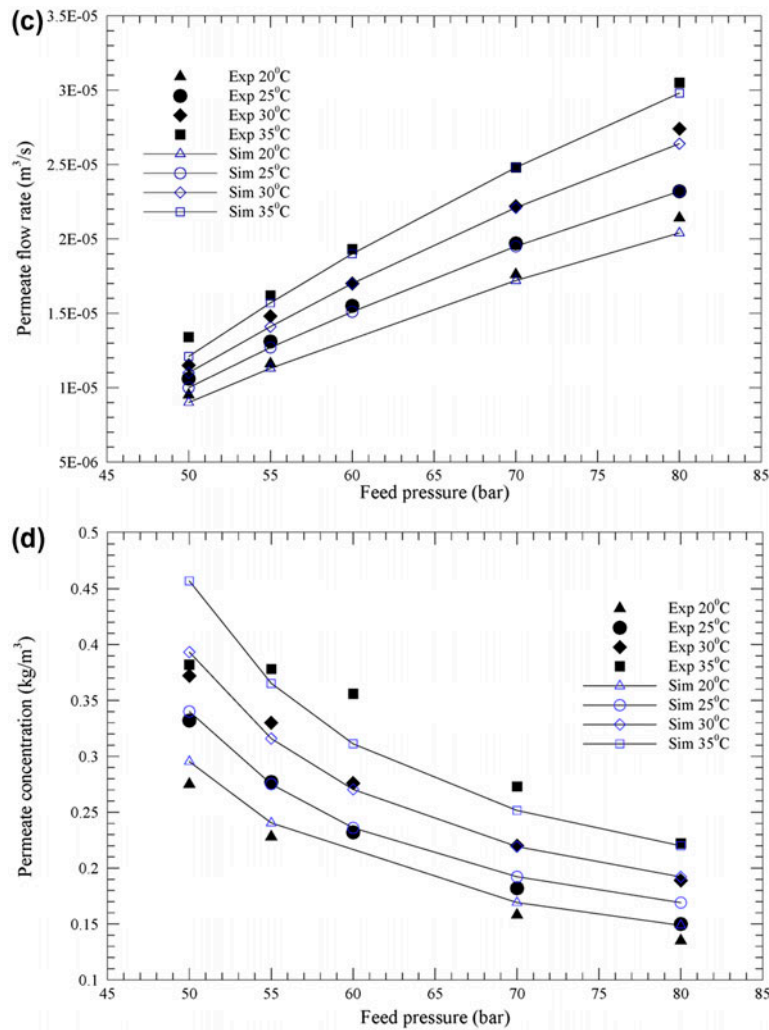


Fig. 4. (Continued).

2.2. Physical property/parameter determination

The mass transfer coefficient was estimated by the following equation:

$$k = 0.753 \left(\frac{K}{(2-K)} \right) \left(\frac{D}{h_b} \right) Sc^{(-1/6)} \left(\frac{Pe \cdot h_b}{L_{mix}} \right)^{0.5} \quad (17)$$

where K is the brine spacer mixing efficiency, D is the diffusion coefficient [$m^2 s^{-1}$; $L^2 T^{-1}$], Schmidt number $Sc = \mu/\rho D$, Peclet number $Pe = h_b U_b/D$, L_{mix} is brine spacer characteristic length [m ; L], μ is dynamic viscosity [$Pa s$; $ML^{-1}T^{-1}$], ρ is density [$kg m^{-3}$; ML^{-3}], h_b is feed channel thickness [m ; L], and U_b is feed solution velocity [$m s^{-1}$; LT^{-1}] ($U_{b_{i+1,j}} = U_{b_{i,j}} - 2\Delta X J_{v_{ij}}/h_b$). The solute diffusion coefficient, viscosity, and density are estimated as follows [19]:

$$D = 6.725 \times 10^{-6} \exp(0.1546 \times 10^{-3}C - 2513/T) \quad (18)$$

$$\mu = 1.234 \times 10^{-6} \exp(0.00212C + 1965/T) \quad (19)$$

$$\rho = 498.4M + \sqrt{248400M^2 + 752.4MC} \quad (20)$$

$$(M = 1.0069 - 2.757 \times 10^{-4}t) \quad (21)$$

where T = feed temperature [K ; θ], and t = relative temperature [$^{\circ}C$; θ], (ratio of feed temperature in ($^{\circ}C$) to ambient temperature ($25^{\circ}C$))

The SWM dimensions and performance parameters are summarized in Table 1.

Table 1
Membrane module characteristics and performance parameters (2.5'' FT30 [8,10])

Parameters	Value
Length of membrane sheet, L (m)	0.854
Width of membrane sheet, W (m)	1.10
Number of leaves per module	1
Feed channel height, h_b (m)	7.7×10^{-4}
Permeate channel height, h_p (m)	4.1×10^{-4}
Friction parameter for feed channel, K_{fb} (m^{-2})	2.5008×10^8
Friction parameter for permeate channel, K_{fp} (m^{-2})	1.2×10^{10}
Efficiency of mixing net, K (dimensionless)	0.5
Characteristic length of spacer, L_{mix} (m)	0.006

2.3. Algorithm to simulate the SWM

The model calculation steps (algorithm) for the prediction of the permeate flow rate (Q_{pt}) and concentration C_{pt} are outlined here.

- Step 1: Assume the solution flux through the membrane (J_v), and permeate concentration (C_p).
- Step 2: Calculate C_b , P_b , and P_p using Eqs. (7), (13), and (14), respectively.
- Step 3: Calculate k , ϕ , and R using Eqs. (17), (5), and (8), respectively.
- Step 4: Calculate J_v Eq. (4) and C_p Eq. (6).
- Step 5: Compare the calculated J_v and C_p (Step 4) with the assumed values. On the convergence of calculated values to respective assumed J_v and C_p values, Go to Step 7 else Go to Step 6.
- Step 6: Assume new J_v and C_p Go to Step 2.
- Step 7: Calculate Q_{pt} and C_{pt} Eqs. (15) and (16).

To execute this algorithm, a computer program in the FORTRAN language was developed.

3. Estimation of permeability

In order to simulate the system behavior, the mathematical model depends on the accuracy of model parameters data which make the mathematical model a useful analysis tool. For the estimation of parameters, the model predictions are compared with experimental data (numerically/graphically). In present work, a numerical approach is considered, because it can simultaneously relate different operating conditions (temperature, pressure, and concentration) with permeability linearly/non-linearly.

The numerical solution (presented in the previous section) was incorporated with the process integration

and design optimization software PIANO (Process Integration, Automation, and Optimization) [20] to study/estimate the permeability correlations. An unconstrained optimization problem was formulated that minimizes the following objective function Eq. (22):

$$F_{obj} = \sum_{i=1}^{NS} \left(\frac{Q_{p,exp,i} - Q_{p,calc,i}}{Q_{p,exp,i}} \right)^2 + \sum_{i=1}^{NS} \left(\frac{C_{p,exp,i} - C_{p,calc,i}}{C_{p,exp,i}} \right)^2 \quad (22)$$

The established optimization procedure was to trace the representative equations for water and salt permeability that minimize the error Eq. (22). Different permeability correlations were used in the numerical model and the prediction of the numerical model (permeate flow rate and concentration) were matched with the experimental readings. The forms of correlations studied were found in published work [9,10,17–19], and also based on intuition. The correlations studied were as follows:

- Water permeability correlations (I to V) studied were:

$$(I) \quad (a_0 + a_1 T^* + a_2 T^{*2}) \times 10^{-12} \exp(-a_3 P)$$

$$(II) \quad a_0 \times 10^{-12} \exp\left(-\frac{a_1}{R} \left(\frac{1}{T} - \frac{1}{T_{rel}}\right)\right)$$

$$(III) \quad a_0 \times 10^{-12} \exp\left(-\frac{a_1}{R} \frac{1}{T}\right)$$

$$(IV) \quad a_0 \times 10^{-12} \left(\frac{T}{T_{rel}}\right) \left(\frac{P}{P_{rel}}\right)$$

$$(V) \quad a_0 \times 10^{-12} \left(\frac{T}{T_{rel}}\right)^{a_1} \left(\frac{P}{P_{rel}}\right)^{a_2}$$

- Salt permeability correlations (VI to XII) studied were:

$$(VI) \quad (b_0 + b_1 T^* + b_2 T^{*2}) \times 10^{-8} \exp(-b_3 P)$$

$$(VII) \quad b_0 \times 10^{-8} \exp\left(-\frac{b_1}{R} \left(\frac{1}{T} - \frac{1}{T_{rel}}\right)\right)$$

$$(VIII) \quad b_0 \times 10^{-8} \exp\left(-\frac{b_1}{R} \frac{1}{T}\right)$$

$$(IX) \quad b_0 \times 10^{-8} \exp\left(b_1 \frac{T^*}{T_{rel}}\right)$$

$$(X) \quad b_0 \times 10^{-8} \exp\left(\frac{b_1 T^*}{T_{rel}} - \frac{b_2}{P} - \frac{b_3}{C}\right)$$

$$(XI) \quad b_0 \times 10^{-8} \exp\left(\frac{b_1 T^*}{T_{rel}} + \frac{b_2}{P} - \frac{b_3}{C}\right)$$

$$(XII) \quad b_0 \times 10^{-12} (P)^{-b_2} \exp(b_1 T^*)$$

For optimization, direct search settings using micro-genetic algorithm [21] was used. Each set of correlations was tried thrice by changing the initial values to find the global optimum instead of local optimum.

4. Results and discussion

The ability of a model to predict the physical phenomena precisely depends on many factors including the assumptions underlying mathematical calculations, and the accuracy of model parameters. For the estimation of pressure drop in a spacer-filled channel, Karode et al. [22] related it to the channel length, feed velocity, density, hydraulic diameter, drag coefficient, and spacer porosity. While Koutsou et al. [23] measured the pressure drop by relating it to diameter of filaments, angle between crossing filaments, channel size, density, and feed flow rate. These studies estimate pressure drop for known geometrical configuration. The flow in spacer-filled channels at low Reynolds number (34–45) is unsteady [23], but in the present study the Reynolds number is lower than this range (14–20). The flow in the present study is not in transition region and the validity of Darcy's law can be safely assumed. Moreover, with the help of this assumption previous numerical studies have shown good agreement with experimental readings [8,10]. Furthermore, the use of Darcy's law in recent published works [11,24–29] in a variety of membrane processes (such as RO, direct contact membrane distillation, pressure retarded osmosis, and vacuum membrane distillation) and the reproduction of experimental data indicate its applicability.

Several authors [8,11,17,30,31] estimated the mass transfer coefficient by establishing a relationship between the Sherwood number, Reynolds number, and Schmidt number. Many of such established relationships are usually limited to that system only. In contrast to many other published mass transfer coefficient relationships, the relation developed by Winograd et al. [30] has been widely used. Many researchers [8,10,19,24] have used this relation for various RO simulation models. The same mass transfer coefficient relation was considered appropriate for this study.

The present study is based on experimental work presented in Ref. [10]. The parameters with constant values (K_{fb} , K_{fp} , K , L_{mix}) used in the present study are based on the same experimental work, so these values were considered sufficient for the present analysis. Moreover, the numerical model presented in Ref. [10] is based on the "solution diffusion model", and that of Ref. [8] is based on a three parameter concept by Spiegler–Kedem. The models based on different membrane transport fundamentals used the same parameter values.

Apart from these parameters, in an RO simulation model, an important parameter, permeability, has a significant effect on the predicted permeate flow rate/concentration, so a thorough examination for its estimation is necessary. Suitable experimental data are required for the estimation of the parameters. The experimental data presented in Ref. [10] covers a wide range of pressure, temperature, concentration, and flow rate. The SWM used for the experiments was a 2.5' FT30 module element with a thin-film composite polyamide membrane. The range of the operating conditions in the experiments was pressure 50–80 bar, flow rate 0.21–0.24 L/s, temperature 20–35°C, and feed salinity 25–35 kg m⁻³ (for further details please refer to Table 1). This experimental data is considered as a benchmark to estimate the permeability. In the present work apart from the permeability, all the physical properties of the feed along with system parameters were known/fixed (as discussed in previous sections). In this setting, the permeability can be studied and estimated reliably.

4.1. The effect of permeability on the model prediction

The numerical procedure presented in Section 2 was used to understand the significance of the water and salt permeability under different operating conditions (50–80 bar, 20–35°C, and 25–35 kg m⁻³). The effects of variation in the permeability under constant operating conditions (20°C, 55 bar, 35 kg m⁻³, and 2.1498 m³/s) are shown in Fig. 3(a) and (b). For these simulations, the salt permeability in Fig. 3 (a) is kept constant (2.76E–8 m/s), and the water permeability in Fig. 3(b) is kept constant (5.25E–12 m³/m²s Pa). It is obvious from these figures that changing the permeability values results in significantly different predicted flow rates and concentration.

4.2. Optimization methodology for the prediction of permeability

The permeability correlations are membrane or application specific. Due to the highly non-linear

behavior of the membrane in different operating conditions, the membrane characteristic (i.e. permeability) is estimated indirectly from the experimental data. The operating condition influences the permeability, and a numerical model can better simulate the RO/SWM with a suitable representation of the membrane permeability in terms of the physical quantities (pressure, temperature, and concentration).

The focus of the above discussion is the estimation of the appropriate parameter to improve the simulation of RO/SWM that can be validated by experimental data. As furnished in the Introduction section, different approaches to estimate the permeability can be used. To trace out the trends that permeability follows under the influence of temperature, pressure, and concentration, in present work, different correlation combinations were studied using the optimization methodology (explained in the previous section). The coefficients of the correlations which minimize Eq. (22) were determined by optimization. The optimum coefficients for different correlation combinations along with relative deviation between the predicted and experimental values of the permeate flow rate and concentration are furnished in Table 2. All the combinations of the correlations presented in Section 3 were studied; however, only some of the important results are summarized in Table 2.

The correlation that gives the minimum relative deviation between the predicted and experimental values is chosen. The outcome of the established optimization procedure was the estimation of water and salt permeability, which are as follows:

- Water permeability correlation:

$$A = (6.252 + 0.00545T^* + 0.00867T^{*2}) \times 10^{-12} \exp(-1.139E - 7 \times P) \tag{23}$$

- Salt permeability correlation:

$$B = 1.0605 \times 10^{-8} \exp\left(\frac{13.55T^*}{T_{rel}} + \frac{1.4551E6}{P} - \frac{10.52}{C}\right) \tag{24}$$

The experimental data analyzed in this paper has wide range feed operating conditions such as temperature (20–35 °C), pressure (50–80 bar), and concentration (25–40 kg m⁻³). By using the mentioned methodology, a single correlation of water permeability/salt permeability applicable over a wide range of operating conditions was determined.

Table 2

Optimized coefficients of the water and salt permeability correlation combinations along with the relative difference in the predicted and experimental results using respective correlations in the numerical model

Correlation combination		a_0	b_0	a_1	b_1	a_2	b_2	a_3	b_3	F_{obj} Eq. (22)
(V) and (XI)	(V)	2.5026	–	3.08002	–	0.1588	–	–	–	1.091
	(XI)	–	1.0689	–	12.7984	–	6.406E5	–	3.999	
(III) and (VIII)	(III)	5.8694	–	57.3044	–	–	–	–	–	3.267
	(VIII)	–	3.7464	–	286.07	–	–	–	–	
(II) and (VII)	(II)	5.7320	–	20.4427	–	–	–	–	–	3.256
	(VII)	–	3.2964	–	371.68	–	–	–	–	
(IV) and (IX)	(IV)	0.0898	–	–	–	–	–	–	–	4.296
	(IX)	–	3.3248	–	19.916	–	–	–	–	
(I) and (VII)	(I)	12.3865	–	0.01130	–	1.57E–5	–	1.239E–7	–	3.175
	(VII)	–	3.3841	–	10.908	–	–	–	–	
(I) and (VI)	(I)	16.2475	–	0.3863	–	0.0733	–	4.08E–7	–	3.734
	(VI)	–	6.2410	–	0.2613	–	1.25E–7	–	2.96E–7	
(I) and (XII)	(I)	12.9329	–	0.0559	–	0.00468	–	1.75E–7	–	2.082
	(XII)	–	1.005	–	0.0166	–	8745E–6	–	–	
(I) and (X)	(I)	8.5435	–	0.0381	–	0.01004	–	1.597E–7	–	2.09
	(X)	–	5.0567	–	25.25	–	3.5055E6	–	21.543	
(I) and (XI)	(I)	6.252	–	5.45E–3	–	8.67E–3	–	1.139E–7	–	0.268
	(XI)	–	1.0605	–	13.55	–	1.4551E6	–	10.52	
(I) and (IX)	(I)	4.0386	–	0.05521	–	0.00648	–	7.9E–8	–	0.468
	(IX)	–	0.8837	–	14.514	–	–	–	–	

4.3. Comparison of the predicted results with the published experimental and simulation data

The SWM simulation results (permeate flow rate and permeate concentration) were obtained using the presently determined permeability Eqs. (23) and (24). These predicted permeate characteristics for 25 kg m^{-3} feed concentration in comparison with published experimental and the simulation data are summarized in Table 3. It is obvious from the table that the permeability correlations determined using the present optimization methodology predicts precisely and accurately.

Using the presently determined permeability correlations, the experimental data for different feed concentrations ($C_f = 35 \text{ kg m}^{-3}$, and 40 kg m^{-3}) was also simulated. The predicted and experimental results are plotted in Fig. 4(a)–(d). It is evident from the figures that the predicted results are in close agreement with the experimental data. The predicted permeate concentration is lower than the experimental data at higher temperature. It may be due to the physical relaxation of the membrane pores at higher temperature. By analyzing the model predictions (using Eqs. (23) and (24)) compared to the experimental observations, it is evident that the numerical model is able to predict the permeate flow rate within a 5% error for 88% of the readings, and the permeate concentration within a 10% error for 92% of the readings. Scrutinizing the published predictions of the permeate flow rate/permeate concentration [8,10] with present permeate characteristics prediction (Table 3, Fig. 4) show that the predictions in this study are far better than both [8] and [10].

This work reduced the magnitude of the percentage error and increased the reliability of the model prediction. The residual sum of the squares as defined by Eq. (22) for the present work is 0.2698, while for Ref. [10] is 0.6154. When the residual sum of the squares for the selected 24 data-sets (simulated by [8]) are analyzed, the error Eq. (22) by [8,10], and the present work are 0.2284, 0.1515, and 0.0967, respectively. Using the optimization methodology, presented in the present work for the prediction of permeability, the percentage improvement in prediction is 56.15% better than [10], and for 24 data-sets 57.66% better than [8]. This shows the significance of present study. The applicability of the predicted permeability correlations are analyzed in the next section.

4.4. Validation of the optimized correlation

In the membrane simulation, the models require different fundamental parameters. These parameters

are obtained from experimental data. Several authors [2,9,11,19] have presented a parameter estimation procedure. However, the reliability of the estimated parameters becomes uncertain with the presence of error in the experimental data that propagates in the simulations. To mitigate this problem, the experimental data ([10]) used for the determination of permeability in the present study were carefully taken with negligible instrumental errors while the parameters were determined by well-fitting of curves in the experimental data [32]. The purpose of the present study is the development of a methodology to reliably interpret the effect of operating conditions on permeability. Therefore, in this study a validation of the optimized correlation is also presented to confirm the reliability of i) methodology used to estimate the permeability and ii) determined permeability correlations.

The experimental data [17] was simulated using the present estimated permeability correlations. The range of the operating conditions, membrane, and the membrane module used in Refs. [10] and [17] was identical except for the range of the feed flow rate. Using the calculation procedure mentioned in Section 2, along with the permeability correlations, Eqs. (23) and (24), the predictions for the permeate characteristics are reported in Table 4. The predicted permeate flow rate was within a 6.2% error for 94% of the readings, and the permeate concentration was within an 8% error for 91% of the readings.

It can be inferred that the predicted results using the permeability correlations established in this work predicts the permeate flow rate and the permeate concentrations in close agreement with the experimental readings. Thus, the water permeability correlation Eq. (23), and the salt permeability correlation Eq. (24) are applicable to a wide range of, pressure (50–80 bar), temperature (20–35°C), concentration (25–40 kg m^{-3}), and feed flow rate ($\sim 7\text{E}-5$ to $\sim 2.4\text{E}-4 \text{ m}^3/\text{s}$) for the same membrane and membrane module.

Using the procedure mentioned in this study, the parameters of a numerical model were studied and determined. The permeability determined from one set of experimental data was used to simulate another set of experimental data with different ranges of feed flow rate. The experimental data were well simulated using this approach. This indicates the practical effectiveness of the present study.

The membrane intrinsic property, permeability, is determined by various different procedures explained in the Introduction section. The focus of the present study was the determination of permeability, numerically. Furthermore, the determined permeability can be reliably used for various operating conditions. The results presented in the present study elaborates that

Table 3
 Permeate characteristics of Boudinar's [10] experimental data predicted using permeability correlations Eqs. (23) and (24) in comparison to the published results [8,10] (for $C_f = 25 \text{ kg m}^{-3}$)

Temp. °C	P_f bar	$Q_f \times 10^5$ m^3/s	Exp. $Q_{pt} \times 10^5$ m^3/s	[10] Results		[8] Results		Present predicted		Exp. C_{pt} kg m^{-3}	[10] Results		[8] Results		Present predicted	
				$Q_{pt} \times 10^5$ m^3/s	% Error	$Q_{pt} \times 10^5$ m^3/s	% Error	$Q_{pt} \times 10^5$ m^3/s	% Error		$Q_{pt} \times 10^5$ m^3/s	% Error	C_{pt} kg m^{-3}	% Error	C_{pt} kg m^{-3}	% Error
20	50	21.772	1.710	1.670	2.34	-	1.8433	-7.80	0.092	0.107	-16.30	-	-	0.0944	-2.61	
20	55	21.983	1.933	1.915	0.93	-	2.0771	-7.45	0.089	0.097	-8.99	-	-	0.0857	3.71	
20	60	22.208	2.158	2.155	0.14	2.286	2.2896	-6.10	0.086	0.089	-3.49	0.0896	-4.19	0.0796	7.44	
20	70	22.632	2.582	2.621	-1.51	-	2.6547	-2.82	0.079	0.078	1.27	-	-	0.0715	9.49	
20	80	23.053	3.003	3.069	-2.20	3.444	2.9486	1.81	0.072	0.071	1.39	0.0702	2.44	0.0666	7.50	
25	50	22.075	2.025	1.886	6.86	-	2.1068	-4.04	0.098	0.123	-25.51	-	-	0.1067	-8.88	
25	55	22.332	2.282	2.164	5.17	2.102	2.3802	-4.30	0.095	0.111	-16.84	0.1051	-10.60	0.0969	-2.00	
25	60	22.580	2.530	2.437	3.68	2.417	2.6286	-3.90	0.089	0.102	-14.61	0.0964	-8.33	0.0899	-1.01	
25	70	23.105	3.075	2.967	3.51	3.027	3.0589	0.52	0.082	0.090	-9.76	0.0834	-1.70	0.0807	1.59	
25	80	23.543	3.495	3.475	0.57	3.626	3.4062	2.54	0.072	0.082	-13.89	0.0753	-4.58	0.0752	-4.44	
30	50	22.403	2.353	2.131	9.43	-	2.4015	-2.06	0.118	0.140	-18.64	-	-	0.1211	-2.63	
30	55	22.673	2.623	2.448	6.67	-	2.7189	-3.66	0.108	0.127	-17.59	-	-	0.1099	-1.76	
30	60	23.010	2.960	2.758	6.82	-	3.0105	-1.71	0.100	0.117	-17.00	-	-	0.1019	-1.90	
35	50	22.717	2.667	2.401	9.97	-	2.7195	-1.97	0.129	0.162	-25.58	-	-	0.1383	-7.21	
35	55	23.073	3.023	2.761	8.67	-	3.0872	-2.12	0.121	0.147	-21.49	-	-	0.1255	-3.72	

Table 4

Permeate characteristics of Avlonitis's [17] experimental data predicted using permeability correlations Eqs. (23) and (24)

Temp. °C	Feed Conc. kg m ⁻³	P _f bar	Q _f × 10 ⁵ m ³ /s	Q _{pt} × 10 ⁵ (Exp.) m ³ /s	Q _{pt} × 10 ⁵ (Predicted) m ³ /s	% Error	C _{pt} (Exp.) kg m ⁻³	C _{pt} (Predicted) kg m ⁻³	% Error
20	25	50	17.266	1.6660	1.7490	-4.98	0.095	0.1026	-8.00
20	25	55	17.500	1.9110	1.9725	-3.21	0.089	0.0935	-5.05
20	25	60	17.705	2.1160	2.1753	-2.80	0.089	0.0870	2.24
20	25	70	18.108	2.5200	2.5262	-0.24	0.079	0.0785	0.63
20	25	80	18.516	2.9290	2.8124	3.98	0.075	0.0733	2.26
20	35	50	16.776	1.1880	1.1149	6.15	0.220	0.2177	1.04
20	35	55	7.102	1.2280	1.0117	17.61	0.248	0.2676	-7.90
20	35	55	12.640	1.3580	1.2293	9.47	0.200	0.2087	-4.34
20	35	55	16.996	1.4080	1.3364	5.08	0.187	0.1867	0.16
20	35	55	21.498	1.4480	1.4178	2.08	0.178	0.1722	3.25
20	35	60	17.206	1.6180	1.5400	4.82	0.166	0.1664	-0.24
20	35	70	17.571	1.9830	1.8968	4.34	0.141	0.1421	-0.78
20	35	80	17.880	2.2910	2.1929	4.28	0.139	0.1284	7.62
20	40	70	17.288	1.7000	1.6275	4.26	0.162	0.1844	-13.82
25	35	60	17.368	1.7800	1.7389	2.30	0.182	0.1898	-4.28
25	35	70	17.786	2.1980	2.1529	2.05	0.146	0.1617	-10.75
25	35	80	18.181	2.5930	2.5004	3.57	0.136	0.1458	-7.20
25	40	60	17.106	1.5180	1.4245	6.15	0.242	0.2568	-6.11
25	40	70	17.490	1.9010	1.8386	3.28	0.200	0.2102	-5.09
25	40	80	17.921	2.3330	2.1913	6.07	0.162	0.1850	-14.19
30	35	60	17.571	1.9830	1.9570	1.31	0.228	0.2172	4.73
30	35	70	18.076	2.4880	2.4373	2.03	0.187	0.1846	1.28
30	35	80	18.485	2.8970	2.8405	1.95	0.162	0.1665	-2.77
30	40	60	17.246	1.6580	1.5915	4.01	0.289	0.2952	-2.14
30	40	70	17.746	2.1580	2.0708	4.04	0.235	0.2404	-2.29
30	40	80	18.191	2.6030	2.4788	4.77	0.207	0.2114	-2.12
35	35	60	17.881	2.2930	2.1919	4.40	0.245	0.2495	-1.83
35	35	70	18.348	2.7600	2.7400	0.72	0.218	0.2122	2.66
35	35	80	18.868	3.2800	3.2095	2.14	0.200	0.1910	4.50
35	40	60	17.460	1.8720	1.7684	5.53	0.368	0.3408	7.39
35	40	70	17.963	2.3750	2.3153	2.51	0.299	0.2769	7.39
35	40	80	18.506	2.9180	2.7876	4.46	0.240	0.2428	-1.16

this parameter estimation methodology is convenient and the determined permeability is reliable.

5. Conclusion

A simple optimization methodology to reliably predict permeability correlations was established. Based on the proposed methodology, permeability is determined for the membrane module. Moreover, the consistency of this approach for parameter estimation is verified by the simulation of experimental data. Using this optimization methodology different form of water and salt permeability can be studied. One correlation is thus chosen for water permeability and salt permeability to describe the membrane permeability behavior relative to temperature, pressure, and

concentration. The determined permeability relations showed an impressive improvement in the model predictions to calculate the permeate flow rate and the permeate concentration. Using the optimization methodology, the permeability correlations (for same membrane and membrane module) valid over wide range of operating conditions can be obtained. The agreement with experimental result is strong evidence that the present methodology provides a realistic approach for the estimation of RO membrane permeability.

A new form for salt permeability was determined that ensued the consistent prediction of the permeate concentration. This new form may be useful to predict the salt permeability (and thus the permeate concentration) for other membranes/modules. This study may also be usefully applied to determine/predict the

permeability trends under the influence of operating conditions.

A number of different numerical models are available in literature for different applications, membranes, and modules. However, the approach developed in this study is not limited to the numerical model used in this study, and SWM. It is unique in the sense that it does not modify the membrane transport equations but considerably improves the simulation of SWM. Using this methodology, any numerical model (for any membrane/module) can be integrated with the optimization tool to reliably determine the membrane intrinsic property over a wide range of operating conditions. This methodology can be used to study the effect of different model parameters (including permeability) on the simulation model output. Additionally, it can estimate the single optimum parameter value or trend (correlations) valid over a wide range of operating conditions.

The estimation of permeability parameter over a wide range of operating conditions helps understanding the effect of the operating conditions on membrane performance. The understanding of the effect of physical condition on membranes may lead to the discovery of new material/improved membrane design producing higher water flux with improved solute rejection.

Acknowledgments

PIAnO related guidance by Dong Hoon Choi (Professor, Division of Mechanical Engineering, Hanyang University) was helpful and is gratefully acknowledged. We thank Dr. Sang Jin Lee (Senior Research Engineer, Energy research department, STX Korea), and Dr. Muhammad Shakaib (Associate Professor, NED University, Pakistan) for helpful comments.

List of symbols

A	— water permeability coefficient ($\text{m}^3/\text{m}^2 \text{ s Pa}$)
B	— solute permeability coefficient (m s^{-1})
C	— concentration of solute (kg m^{-3})
D	— diffusivity of solute ($\text{m}^2 \text{ s}^{-1}$)
F	— flow parameter defined by Eq. (12)
h	— height of channel (m)
J_v	— solution flux through membrane ($\text{m}^3/\text{m}^2 \text{ s}$)
k	— mass transfer coefficient (m s^{-1})
K	— mixing efficiency of net
k_{fb}	— brine side friction parameter (m^{-2})
k_{fp}	— permeate side friction parameter (m^{-2})
L	— length of membrane (m)
L_{mix}	— characteristic length of mixing net (m)
m	— divisions along x direction
n	— divisions along y direction
NS	— total number of data sets

N_L	— number of membrane leaves in a module
P	— pressure (Pa)
P_{rel}	— relative pressure (1.01325×10^5 Pa)
Q	— flow rate ($\text{m}^3 \text{ s}^{-1}$)
R	— rejection
S	— membrane surface area (m^2)
T	— feed temperature (K)
T_{rel}	— relative temperature (273.15 K)
T^*	— $T - T_{\text{rel}}$
U	— solution velocity (m/s)
W	— width of membrane (m)
$\Delta x, \Delta y$	— dimension of sub elements along x and y direction (m)

Subscripts

b	— bulk solution side
f	— input feed
i, j	— i th, j th component
m	— membrane feed interface
p	— permeate side
t	— total

Greek letters

α	— osmotic pressure proportionality = $2RT$
μ	— viscosity (kg/m s)
ρ	— density (kg m^{-3})
φ	— concentration polarization
σ	— reflection coefficient

References

- [1] A.D. Khawaji, I.K. Kutubkhanah, J.-M. Wie, Advances in seawater desalination technologies, *Desalination* 221 (2008) 47–69.
- [2] L.-Y. Hung, S.J. Lue, J.-H. You, Mass-transfer modeling of reverse-osmosis performance on 0.5–2% salty water, *Desalination* 265 (2011) 67–73.
- [3] N. Ghaffour, T.M. Missimer, G.L. Amy, Technical review and evaluation of the economics of water desalination: Current and future challenges for better water supply sustainability, *Desalination* 309 (2013) 197–207.
- [4] M.G. Buonomenna, Nano-enhanced reverse osmosis membranes, *Desalination* 314 (2013) 73–88.
- [5] K.C. Ng, K. Thu, Y. Kim, A. Chakraborty, G. Amy, Adsorption desalination: An emerging low-cost thermal desalination method, *Desalination* 308 (2013) 161–179.
- [6] A. Zhu, P.D. Christofides, Y. Cohen, Minimization of energy consumption for a two-pass membrane desalination: Effect of energy recovery, membrane rejection and retentate recycling, *J. Membr. Sci.* 339 (2009) 126–137.
- [7] A. Zhu, P.D. Christofides, Y. Cohen, Energy consumption optimization of reverse osmosis membrane water desalination subject to feed salinity fluctuation, *Ind. Eng. Chem. Res.* 48 (2009) 9581–9589.
- [8] S. Senthilmurugan, A. Ahluwalia, S.K. Gupta, Modeling of a spiral-wound module and estimation of model parameters using numerical techniques, *Desalination* 173 (2005) 269–286.

- [9] S. Avlonitis, W.T. Hanbury, M.B. Boudinar, Spiral wound modules performance. An analytical solution, part I, *Desalination* 81 (1991) 191–208.
- [10] M.B. Boudinar, W.T. Hanbury, S. Avlonitis, Numerical simulation and optimisation of spiral-wound modules, *Desalination* 86 (1992) 273–290.
- [11] S. Sundaramoorthy, G. Srinivasan, D.V.R. Murthy, An analytical model for spiral wound reverse osmosis membrane modules: Part I—Model development and parameter estimation, *Desalination* 280 (2011) 403–411.
- [12] G. Srinivasan, S. Sundaramoorthy, D.V.R. Murthy, Separation of dimethyl phenol using a spiral-wound RO membrane—Experimental and parameter estimation studies, *Desalination* 243 (2009) 170–181.
- [13] K.K. Sirkar, P.T. Dang, G.H. Rao, Approximate design equations for reverse osmosis desalination by spiral-wound modules, *Ind. Eng. Chem. Process Des. Dev.* 21 (1982) 517–527.
- [14] A. Altaee, Computational model for estimating reverse osmosis system design and performance: Part-one binary feed solution, *Desalination* 291 (2012) 101–105.
- [15] Y. Liu, X. Chen, High permeability and salt rejection reverse osmosis by a zeolite nano-membrane, *PCCP* 15 (2013) 6817–6824.
- [16] G.M. Geise, H.B. Park, A.C. Sagle, B.D. Freeman, J.E. McGrath, Water permeability and water/salt selectivity tradeoff in polymers for desalination, *J. Membr. Sci.* 369 (2011) 130–138.
- [17] S. Avlonitis, W.T. Hanbury, M.B. Boudinar, Spiral wound modules performance an analytical solution: Part II, *Desalination* 89 (1993) 227–246.
- [18] N.G. Voros, Z.B. Maroulis, D. Marinos-Kouris, Salt and water permeability in reverse osmosis membranes, *Desalination* 104 (1996) 141–154.
- [19] P.P. Mane, P.-K. Park, H. Hyung, J.C. Brown, J.-H. Kim, Modeling boron rejection in pilot- and full-scale reverse osmosis desalination processes, *J. Membr. Sci.* 338 (2009) 119–127.
- [20] PIAO (Process Integration, Automation and Optimization) User's Manual, Version 3.3, PIDOTECH, Seoul, 2011, pp. 155–156.
- [21] K. Krishnakumar, Micro-genetic algorithms for stationary and non-stationary function optimization, in: 1989 Advances in Intelligent Robotics Systems Conference, International Society for Optics and Photonics, Philadelphia, PA, 1990, pp. 289–296.
- [22] S.K. Karode, A. Kumar, Flow visualization through spacer filled channels by computational fluid dynamics I: Pressure drop and shear rate calculations for flat sheet geometry, *J. Membr. Sci.* 193 (2001) 69–84.
- [23] C.P. Koutsou, S.G. Yiantsios, A.J. Karabelas, Direct numerical simulation of flow in spacer-filled channels: Effect of spacer geometrical characteristics, *J. Membr. Sci.* 291 (2007) 53–69.
- [24] P.-K. Park, S. Lee, J.-S. Cho, J.-H. Kim, Full-scale simulation of seawater reverse osmosis desalination processes for boron removal: Effect of membrane fouling, *Water Res.* 46 (2012) 3796–3804.
- [25] G. Srinivasan, S. Sundaramoorthy, D.V.R. Murthy, Validation of an analytical model for spiral wound reverse osmosis membrane module using experimental data on the removal of dimethylphenol, *Desalination* 281 (2011) 199–208.
- [26] M. Kostoglou, A.J. Karabelas, Comprehensive simulation of flat-sheet membrane element performance in steady state desalination, *Desalination* 316 (2013) 91–102.
- [27] S. Shanmuganathan, T.V. Nguyen, W.G. Shim, J. Kandasamy, S. Vigneswaran, Performance of submerged membrane—Ion exchange hybrid system with PuroLite A502PS in treating reverse osmosis feed, *Sep. Purif. Technol.* 122 (2014) 24–31. Available from: <http://dx.doi.org/10.1016/j.seppur.2013.10.039>
- [28] Q. She, D. Hou, J. Liu, K.H. Tan, C.Y. Tang, Effect of feed spacer induced membrane deformation on the performance of pressure retarded osmosis (PRO): Implications for PRO process operation, *J. Membr. Sci.* 445 (2013) 170–182.
- [29] Ó. Andrjesdóttir, C.L. Ong, M. Nabavi, S. Paredes, A.S.G. Khalil, B. Michel, D. Poulikakos, An experimentally optimized model for heat and mass transfer in direct contact membrane distillation, *Int. J. Heat Mass Transfer* 66 (2013) 855–867.
- [30] Y. Winograd, A. Solan, M. Toren, Mass transfer in narrow channels in the presence of turbulence promoters, *Desalination* 13 (1973) 171–186.
- [31] M. Khayet, J.I. Mengual, Effect of salt type on mass transfer in reverse osmosis thin film composite membranes, *Desalination* 168 (2004) 383–390.
- [32] S. Avlonitis, Personal Communication. Technological Educational Institute of Chalkida, Chalkida, 2013.